STRUCTURAL BIOLOGY

The structure of a membrane adenylyl cyclase bound to an activated stimulatory G protein

Chao Qi[1,2], Simona Sorrentino[3], Ohad Medalia[3,4], Volodymyr M. Korkhov[1,2]*

Membrane-integral adenylyl cyclases (ACs) are key enzymes in mammalian heterotrimeric GTP-binding protein (G protein)–dependent signal transduction, which is important in many cellular processes. Signals received by the G protein–coupled receptors are conveyed to ACs through G proteins to modulate the levels of cellular cyclic adenosine monophosphate (cAMP). Here, we describe the cryo–electron microscopy structure of the bovine membrane AC9 bound to an activated G protein αs subunit at 3.4-angstrom resolution. The structure reveals the organization of the membrane domain and helical domain that spans between the membrane and catalytic domains of AC9. The carboxyl-terminal extension of the catalytic domain occludes both the catalytic and the allosteric sites of AC9, inducing a conformation distinct from the substrate- and activator-bound state, suggesting a regulatory role in cAMP production.

Membrane-integral adenylyl cyclases (ACs) are key proteins in mammalian signal transduction, responding to a large array of extracellular and intracellular cues and generating cyclic adenosine monophosphate (cAMP) for a range of downstream signaling events (*1*, *2*). The membrane ACs integrate multiple signaling cascades—for example, linking the inputs from G protein–coupled receptors (GPCRs), changes in intracellular Ca^{2+} concentrations (*3*), and lipid signaling cascades (*4*). There are nine AC subtypes in mammals, classified as AC1 to AC9 (*5*). On the basis of amino acid sequence, all of the AC subtypes share the same overall predicted architecture. They are polytopic membrane proteins, composed of 12 transmembrane (TM) helices and featuring cytosolic N and C termini. The first six TM domains (TM1–TM6) of the AC polypeptide are followed by a cytosolic region that includes a catalytic domain (C1a), followed by a C1b domain, the second TM region, the TM7–TM12 bundle, and then a second catalytic domain (C2a) and a C-terminal C2b domain. The N- and C-terminal portions of the proteins are highly variable, whereas the most conserved portions are the C1a and C2a domains, which belong to the class III nucleotidyl cyclases (*5*, *6*). X-ray crystallography of a chimeric $AC5_{C1}/AC2_{C2}$ in a complex with the stimulatory G protein subunit Gαs (*7*, *8*) revealed the key features of the AC catalytic machinery and helped in the formulation of a detailed mechanism of cAMP production by the G protein–dependent ACs (*7*, *8*). However, each of the mammalian membrane ACs includes additional structural elements, such as the membrane-spanning domain and the helical domain (HD), which are critical for the correct assembly of these proteins and for their enzymatic function.

With the cloning of the first mammalian AC came the suggestion that ACs may resemble transporters (*9*). Early studies of ACs in *Paramecium* suggested that the TM portion of the protein may have an ion channel function (*10*). Consistent with their channel function, the sequence of the *Paramecium* AC TM portion is homologous to that of voltage-gated potassium channels (*11*). The presence of a polytopic TM helix bundle and the cytosolic adenosine 5′-triphosphate (ATP)–binding domain hint at a superficial structural and functional similarity to the ATP-binding cassette (ABC) transporters. However, there is no substantial sequence similarity between ACs and any known transporter-like or ion channel–like proteins. Studies of mycobacterial and mammalian ACs indicated a possible role of the TM domains in the correct assembly of the enzyme (*7*, *12*, *13*). However, the structural and functional role of the TM region remains unclear.

AC9 is a cyclase subtype expressed in many tissues, including lung, brain, and heart (*14*, *15*). It has been extensively studied in conjunction with A-kinase anchoring protein (AKAP) complexes (*16*). It has been proposed that AC9 is linked through the AKAP Yotiao with I_{Ks} potassium channels, protein kinase A, phosphodiesterase PDE4D3, and protein phosphatase PP1 (*17*). AC9 has been identified as a potential drug target in asthma (*5*). rs2230739, a polymorphism of AC9 that results in an $Ile^{772}\rightarrow Met$ mutation, is associated with changes in response to the inhaled corticosteroid budesonide (*18*). In a canonical model of AC activation, forskolin binds to an allosteric site adjacent to the catalytic site, leading to activation of the enzyme. Interaction between the AC and Gαs subunit in a guanosine 5′-triphosphate (GTP)–bound state also leads to AC activation, with maximal AC activation achieved in the presence of both the forskolin and the Gαs protein. However, although sequence comparisons with other ACs show that AC9 contains an allosteric site and one previous report suggested that forskolin can activate AC9 (*14*), several studies concluded that AC9 is forskolin insensitive and the consensus in the field has been that AC9 stands in its own category as a forskolin-insensitive protein (*19*, *20*).

The ACs have long remained a missing piece in our understanding of signal transduction, possibly because of the recognized difficulties in expressing and purifying these proteins for biochemical and structural studies (*21*). To fill this gap, we determined the structure of the bovine AC9 in complex with Gαs (AC9-Gαs) using cryo–electron microscopy (cryo-EM) and single-particle analysis.

We expressed and purified the bovine AC9 (fig. S1A) and confirmed its functional integrity using cAMP accumulation assays (Fig. 1, A to C). The purified protein catalyzed the conversion of ATP into cAMP and could be inhibited by MANT-GTP (2′-/3′-*O*-(*N*′-methylanthraniloyl)guanosine-5′-*O*-triphosphate), an inhibitory AC substrate analog (Fig. 1B). Reconstitution of the protein with the GTPγS-activated Gαs (fig. S1, B and C) led to a robust activation of the cyclase (Fig. 1A). Tests of the ability of the universal AC activator forskolin to activate the AC9 in vitro revealed a very weak activation of the AC9 at submillimolar concentrations (Fig. 1A). By contrast, forskolin could activate the AC9-Gαs complex with a median effective concentration (EC_{50}) of 111 μM (Fig. 1A and table S2). Thus, although both forskolin and the Gαs subunit were capable of partially activating the protein, full activation could be reached only by combining the two agents. Moreover, as expected from an allosteric modulator of the AC, forskolin shifted the median inhibitory concentration (IC_{50}) of the AC9 substrate analog MANT-GTP toward the lower concentration (Fig. 1, B and C). Therefore, our in vitro experiments using purified full-length AC9 and Gαs protein clearly show that forskolin acts on the AC9-Gαs protein complex as a classical allosteric activator.

We prepared frozen, hydrated cryo-EM grids containing the AC9-Gαs complex in the presence of MANT-GTP and forskolin at concentrations (0.5 mM for each ligand) exceeding the IC_{50} and EC_{50} values for these two compounds and subjected them to single-particle cryo-EM analysis (fig. S2). The best subset of particles resulted in a density map corresponding to the complete complex of the cyclase and G protein subunit, refined to a resolution of 3.4 Å (Fig. 1D). The complete density map, together with the maps obtained after focused refinement of the membrane-embedded (fig. S3) and cytosolic (fig. S3) parts of the complex, allowed us to build a complete three-dimensional (3D) model of the AC9-Gαs complex (Fig. 1E). The map and the model revealed

[1]Institute of Biochemistry, ETH Zurich, Zurich, Switzerland. [2]Laboratory of Biomolecular Research, Division of Biology and Chemistry, Paul Scherrer Institute, Villigen, Switzerland. [3]Institute of Biochemistry, University of Zurich, Zurich, Switzerland. [4]Department of Life Sciences and the National Institute for Biotechnology in the Negev, Ben Gurion University of the Negev, Beer-Sheva, Israel.
*Corresponding author. Email: volodymyr.korkhov@psi.ch

several key elements of the AC9-Gαs complex: (i) the 12-TM domain bundle of AC9, (ii) the HD connecting the TM bundle and the catalytic domain of AC9, and (iii) the catalytic domain of AC9, bound to the GTPγS-activated Gαs subunit (Fig. 1, D and E, and fig. S6).

The TM domain of the protein possesses a pseudo-twofold symmetry, a feature often found in solute transporters of the resistance nodulation division, ABC, or major facilitator family (Fig. 2, A to C). The transmembrane helices TM1–TM6 and TM7–TM12 can be superposed with a root mean square deviation (RMSD) of 3.4 Å over 176 residues (Fig. 2D). The internal pseudosymmetry supports the hypothesis that the mammalian membrane ACs arose by a gene duplication event from a simple system, possibly similar to that of the "half-cyclase" Cya/Rv1625c from *Mycobacterium tuberculosis* (*12*). The interface between the two TM halves of AC9 is formed by helices TM1, TM4, and TM6 in the N-terminal "half" of the TM domain bundle and TM7, TM10, and TM12 in the C-terminal portion of the protein (Fig. 2, B and C). The cloning of the first mammalian AC gene was accompanied by a suggestion that ACs may act as transporters, based on their primary sequence (*9*). Our structure does not reveal any obvious putative solute translocation pathway within the TM domain bundle, with the TM helices of AC9 packed closely together. Although a digitonin micelle likely provides an environment similar to that of the lipid bilayer, it is possible that the conformation of the TM helices in the physiological environment of the membrane is different.

The TM6 and TM12 helices of AC9 extend into the cytosol, forming 40-residue-long HDs referred to here as HD1 (including helices h1.1 and h2.1) and HD2 (helices h2.1 and h2.2; Fig. 2, E and F). This region is important for the function of ACs and guanylyl cyclases in prokaryotes and eukaryotes (*12*). Residues Leu^{323} to Met^{333} of helix h1.1 and Ile^{1022} to Leu^{1032} of helix h2.1 form a classic coiled coil (Fig. 2F). We previously described the HD of Cya, a membrane AC from *Mycobacterium intracellulare* homologous to the *M. tuberculosis* Rv1625c (*12*). The AC9 HD shows some differences compared with Cya in the relative arrangement of the core region at the boundary with the catalytic domain (Fig. 2, E and F, and fig. S7, A and B). In *M. intracellulare* Cya, the short helices are tightly bound at the C terminus of the coiled coil (fig. S7B). By contrast, the coiled coil of the AC9 unwinds at the C-terminal ends of h1.1 and h2.1 (Fig. 2F, fig. S7B, and fig. S8A). This region of the enzyme is critical for the function of ACs and guanylyl cyclases. Genetic disease–linked mutations map to the HDs of AC5 in familial dyskinesia and facial myokymia (*22*, *23*) and to those of retinal guanylyl cyclase (retGC1) in Leber's congenital amaurosis-1 (*24*) and cone–rod dystrophy-6 (CORD6) (*25*). We can now refine the positions of the disease-linked mutations using the structure of bovine AC9, a much closer approximation to the human pathology–linked nucleotidyl cyclases compared with the *M. intracellulare* Cya.

The function of the 12-TM bundle in mammalian ACs has been unclear. Recent studies in the mycobacterial Rv1625c suggested a possible receptor function for the membrane-spanning region of the mycobacterial homolog (*12*). We could not resolve parts of the extracellular surface of the AC9 (Fig. 2, A and B), and it is not clear whether the membrane-bound

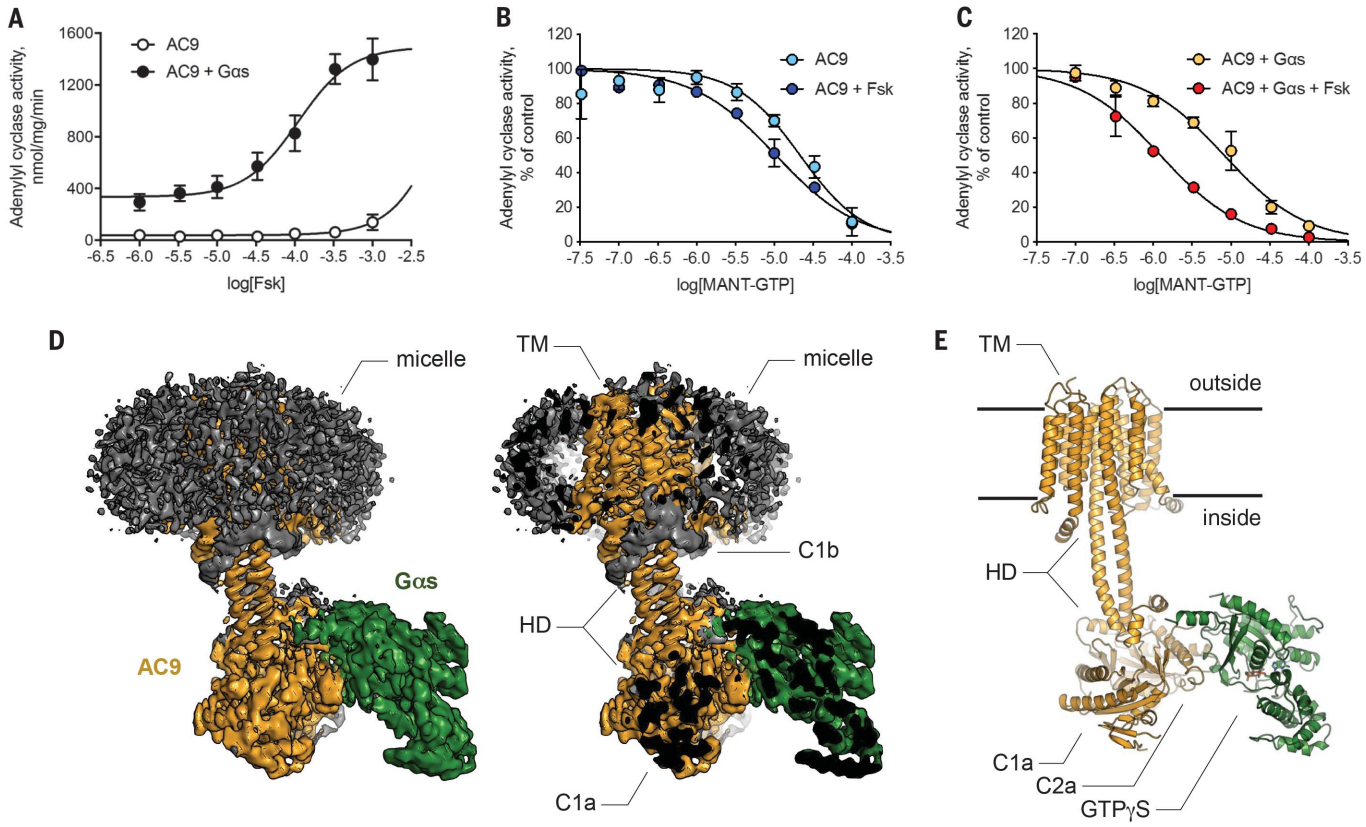

Fig. 1. Function and structure of the AC9-Gαs complex. (**A**) AC activity assays (based on [^{3}H] cAMP determination) show that AC9 is activated by Gαs in vitro and is further stimulated by forskolin (Fsk) only when bound to the Gαs subunit. (**B** and **C**) MANT-GTP inhibition assays of AC9 (B) and AC9-Gαs (C) in the absence and in the presence of forskolin (0.5 mM). (**D** and **E**) Cryo-EM density map of the AC9-Gαs complex (D) allowed us to build the complete molecular model of the complex (E), revealing its key structural elements: the transmembrane domain bundle (TM), the helical domain (HD), the catalytic domain of AC9 (C2a), and the Gαs protein (Gαs). The density map and model elements corresponding to AC9 and the Gαs proteins are colored orange and green, respectively. Detergent and unassigned protein density are colored gray. For illustration purposes, (D) shows the refined map at 3.6-Å resolution featuring a strong density for the detergent micelle.

part of the protein harbors functionally relevant binding sites for hypothetical ligands. Similarly, the C1b domain that links the catalytic domain C1a with the TM7 could not be resolved in our reconstruction (fig. S6, E to G). However, our structure provides clues as to how interactions with the membrane-spanning region could influence the catalytic function of the protein. The helices TM6 and TM12 are continuous with h1.1 and h2.1 in the HD. TM6 and TM12 are located at the interface of the TM1–TM6 and TM7–TM12 helical bundles and are laterally exposed to the lipid bilayer (Fig. 2E and fig. S8B). It is conceivable that direct interactions of TM6 or TM12 with lipids, small molecules, or other proteins could directly influence the catalytic domain by altering the orientation of helices h1.1 and h2.1 (fig. S8B).

The complete AC9 catalytic domain is composed of two halves, C1a and C2a (Figs. 1E and 3A), similar to the previously solved x-ray structures of the soluble domains of membrane ACs (fig. S7, A and C). As was shown previously, the main interaction interface between the G protein α subunit and the AC9 catalytic domain is formed by the insertion of the Gαs Switch II helix into the groove formed by the helices α′2 and α′3 of the AC9 C2a domain (fig. S7, D to F). The HD region h1.2 (residues 340 to 360) is in proximity with the Gαs-interacting surface (fig. S7E). This region of the protein appears to be highly dynamic, and we could not resolve the residues connecting His^{361} and Pro^{384} of AC9 (fig. S7E). Nevertheless, the proximity of this region to the G protein–AC interface suggests that this element of the AC9 structure likely contributes to the interaction between AC9 and Gαs.

A strong-density element located within the ATP-binding site and the forskolin site was detected (Fig. 3, A and B, and fig. S9, A to C). This density showed superficial similarity to MANT-GTP density but did not match its expected location (Fig. 3A). The density in the forskolin site appeared to overlap with the expected position of forskolin (Fig. 3A). A similar density feature was present in the map reconstructed from images of the sample devoid of forskolin (Fig. 3B and fig. S9B). Therefore, independent of the presence of MANT-GTP and/or forskolin, the active and allosteric sites appear to be occupied by a density consistent with a peptide (Fig. 3, A and B, and fig. S9, A and B). Focused 3D classification and refinement revealed a link between this density and the C-terminal region of the C2a domain of AC9 (Fig. 3C and figs. S3 and S9C). Although the density features in this less-populated 3D class (SOL-C map, calculated with only 16,343 particles) are not sufficiently strong to confidently build an atomic

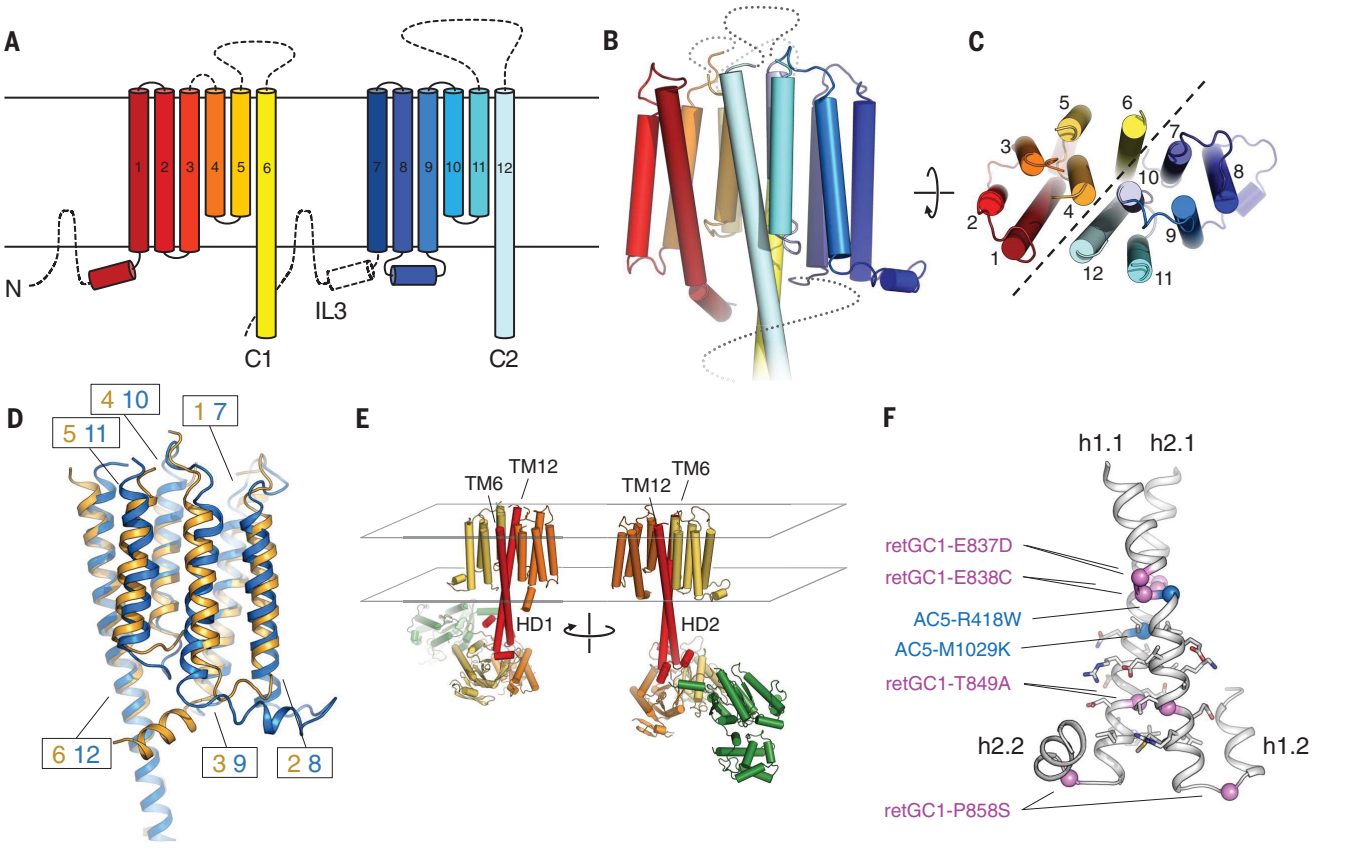

Fig. 2. Structure of the membrane-spanning region and the HD of AC9. (**A**) Topology of the TM domain revealed by the cryo-EM structure. The dotted lines indicate regions that were either absent in the density map (extracellular loops) or present as poorly defined density not amenable to model building. (**B** and **C**) The membrane-embedded portion of AC9 is composed of two pseudosymmetric halves (TM1–TM6 and TM7–TM12); the arrangement of the corresponding helices within these two halves is nearly identical (i.e., TM1–TM7, TM2–TM8, etc.). The helices are packed tightly, and the structure shows no substantial cavity of a translocation pathway to suggest a transport function. The dashed lines indicate elements of the structure that could not be built due to poor-density map features (B). (**D**) The two halves of the membrane-embedded part of bovine AC9 (TM1–TM6 and TM7–TM12) can be structurally superposed with RMSD of 3.4 Å. (**E**) TM1–TM5 (orange) and TM7–TM11 (yellow) regions of AC9 envelope the key TM6/TM12, likely providing the necessary constraints for correct positioning of these two helices. The helices TM6 and TM12 extend into the cytosol and become the two helices h1.1 and h2.1 of HD1 and HD2 (red). (**F**) The HD is stabilized by an 11-residue coiled coil indicated by stick representation of the amino acid side chains, which are labeled as "cc." The HDs of the homologous human cyclases AC5 and retinal guanylyl cyclase (retGC1) have been shown to harbor disease-linked mutations. Mutations in AC5 linked to familial dyskinesia with facial myokymia are indicated as blue spheres; those in retGC1, linked to Leber's congenital amaurosis-1, and CORD6 are shown as violet spheres.

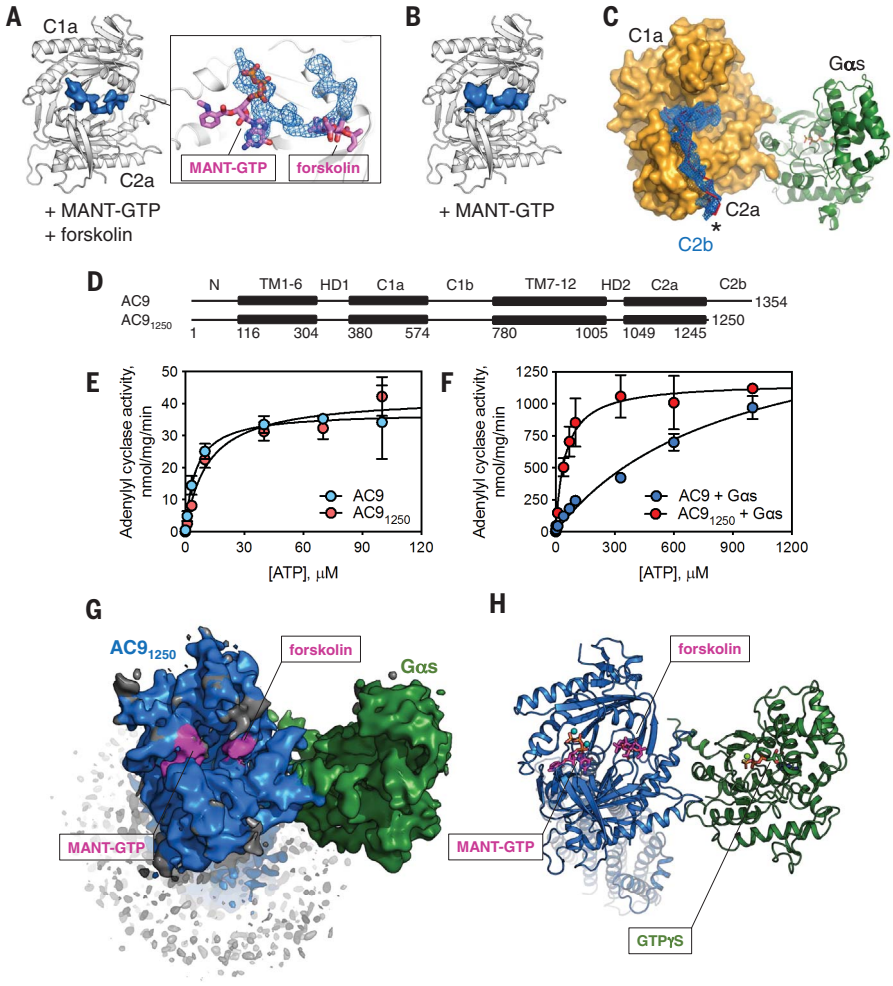

Fig. 3. The structure of Gαs-bound AC9 represents a previously undescribed occluded conformation. (**A**) View of the AC9 catalytic domain overlaid with the density occluding the nucleotide and forskolin-binding site (SOL map, marine). The expected positions of MANT-GTP and forskolin are based on the x-ray structure of $AC5_{C1}/AC2_{C2}$/Gαs (Protein Data Bank ID: 1U0H). (**B**) A similar view of the occluding density in the soluble domain cryo-EM map in the absence of forskolin (SOL-M map). (**C**) The occluding density is clearly linked to the C terminus of the C2a domain (asterisk) in the SOL-C density map (C2b, blue mesh; Cα, red). (**D**) Domain organization of AC9 and the truncated $AC9_{1250}$ construct. (**E**) Wild-type and truncated AC9 variants showing similar enzymatic activity in the absence of G protein. (**F**) Both AC9 and $AC9_{1250}$ are potently stimulated by the GTPγS-activated Gαs, with $AC9_{1250}$ showing a significantly reduced K_m for ATP. (**G**) A 3D reconstruction of the $AC9_{1250}$-Gαs bound to MANT-GTP and forskolin ($AC9_{1250}$-Gαs-MF) shows a density for the two ligands (magenta). (**H**) Same view of the model of the $AC9_{1250}$-Gαs-MF complex.

protein model, using the available density as a constraint, we could assign it to residues Cys^{1246} to Pro^{1275} of the AC9 C terminus, or C2b domain (Fig. 3C and fig. S9C). The high quality of the density inside the allosteric and the active site (Fig. 3A and fig. S9, A and D) allowed us to build the model of the occluding peptide, corresponding to residues Ile^{1263} to Pro^{1275} of the C2b domain of AC9 (fig. S9D). This region is highly conserved among the vertebrate AC9 homologs (fig. S9E) but not in the other AC isoforms (AC1 to AC8) (fig. S10).

To determine the functional role of the C2b domain in AC9, we compared the enzymatic properties of the wild-type and the truncated protein devoid of the C2b domain $AC9_{1250}$ (Fig. 3D and fig. S11A). The two constructs showed comparable ability to convert ATP to cAMP, with similar Michaelis constant (K_m) and V_{max} values (Fig. 3E and table S2). $AC9_{1250}$ was activated by forskolin and inhibited by MANT-GTP in a manner similar to that of AC9 (fig. S11, B to D). Addition of Gαs potently stimulated cAMP production by AC9 (Fig. 3F), with a concomitant increase in its K_m for ATP. Consistent with the tail inhibiting ATP binding, $AC9_{1250}$ showed a high V_{max} but at a much lower K_m value (Fig. 3F). This is a strong indication that the C2b region plays a functional role in the G protein–bound state of AC9. Removal of the C2b region increases the affinity of AC9 for ATP in the presence of Gαs, allowing the protein to reach a maximal rate of catalysis at much lower ATP concentrations. Reduction of the affinity for the substrate (ATP) by occlusion of the active site by the C2b domain may represent a regulatory mechanism for controlling cAMP production by the G protein–bound AC9.

To assess the conformational changes in the occluded state of AC9, we determined the cryo-EM structure of the $AC9_{1250}$-Gαs complex in the presence of MANT-GTP and forskolin ($AC9_{1250}$-Gαs-MF; Fig. 3, G and H, and figs. S12 and S13). The reconstruction at 4.2-Å resolution allowed us to clearly resolve the density for MANT-GTP and forskolin bound at their canonical binding sites (Figs. 3, G and H, and 4; fig. S13, E to G). Comparison of the catalytic domain arrangement of the $AC9_{1250}$-Gαs-MF and AC9-Gαs complexes revealed a small relative rearrangement of the C1a dependent on the presence of the occluding peptide in the active and allosteric sites (Fig. 4, A and B); the RMSD between the atoms of the mobile C1a domains (Ile^{1380} to Gln^{574}) of the two compared structures aligned using their C2a domains (Gln^{1049} to Lys^{1245}) is 1.9 Å. The subtle whole-domain movement observed in the occluded state of AC9 shifts the amino acid residues of C1a involved in nucleotide binding by ~3 Å (fig. S13H). Therefore, the core catalytic domain of AC9 adopts an occluded conformation, with the C2b-derived peptide occupying the active and allosteric sites of the protein (fig. S9, D and E) concomitant with a distortion of the active site compared with that observed in the MANT-GTP– and forskolin-bound state.

The structure of the AC9-Gαs complex in an occluded conformation allowed us to revisit the established model of cAMP-based signal transduction (*7*, *26*) (fig. S14). Activation of the GPCR cascade must lead to formation of the Gαs subunit–bound form of the AC to generate cAMP. However, the occluded state described here adds an intermediate that has previously not been appreciated. The occluded state and the active state of AC9 likely exist in an equilibrium; the sample that produced the reconstruction of the occluded state can be activated by G protein and can produce cAMP. The substantially reduced K_m of the protein for ATP (Fig. 3F) further

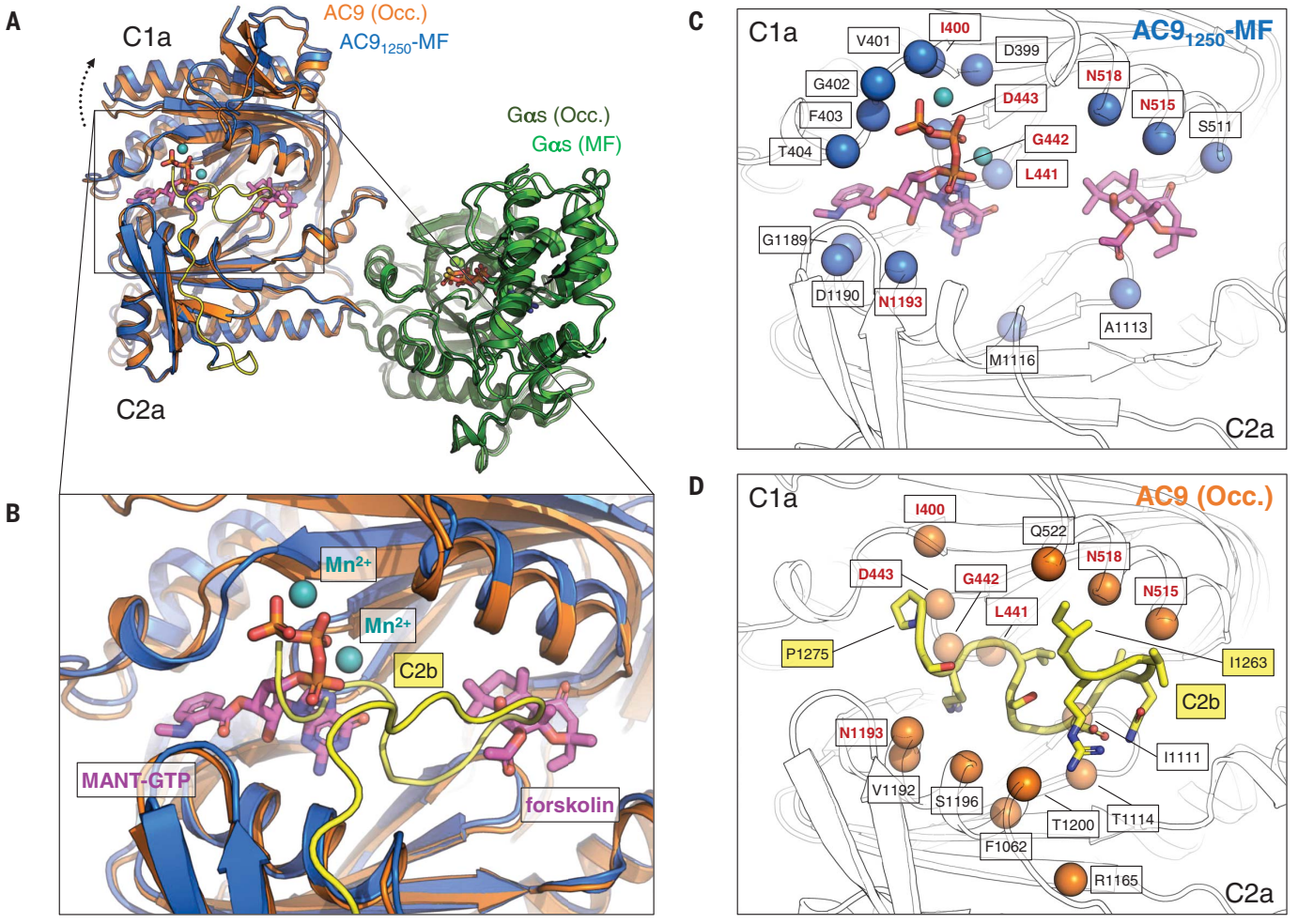

Fig. 4. Comparison of the occluded and nucleotide and forskolin states of the AC9-Gαs complex. (**A** and **B**) Arrangement of the AC9 C1a domain in the occluded state ["AC9 (Occ.)," orange] and in the nucleotide- and forskolin-bound state ("AC9$_{1250}$-MF," blue) based on the corresponding cryo-EM structures. Structural alignment was performed using the C2a domains. The relative C1a domain displacement is indicated by a dotted arrow. The C2b domain is indicated as a cartoon colored yellow in (B). (**C**) Cα atoms of residues within 3.5 Å of the MANT-GTP/2Mn^{2+} and forskolin in AC9$_{1250}$ are shown as blue spheres. (**D**) Cα atoms of residues within 3.5 Å of the occluding peptide (residues Ile^{1263} to Pro^{1275}) in AC9 are shown as yellow spheres. Residues within 3.5 Å of the ligands and the peptide in both structures in (C) and (D) are indicated with red labels.

suggests that occlusion of the ATP site may be favored in the presence of the G protein. Future experiments will help to define the functional role of this protein conformation in the catalytic cycle of AC9.

The architecture of AC9 revealed in this study provides clues to the possible role of the membrane-embedded parts in mammalian ACs. One apparent function of the membrane domain is to enable the correct assembly of the active cyclase. This is accomplished by TM6 and TM12 providing the frame for the HD. It is likely that the elements of the protein that cannot presently be resolved, i.e., the N terminus and the C1b domain, contribute to the assembly and regulation of the cyclase function of AC9 (fig. S6, E to G). Therefore, despite the separation of the catalytic domain by ~40 Å from the lipid bilayer, it is conceivable that the membrane portion of the protein can influence the catalytic domain via the HD and the loop regions adjacent to it.

The occluded state of the complex with the C-terminal peptide binding both the active and the allosteric site of the AC9 may represent an important autoregulatory mechanism built into the AC-based signal transduction machinery. The presence of the peptide may help to explain the inconsistent observations of forskolin insensitivity of AC9 (*14*, *19*, *20*), supporting context-dependent autoregulation of AC9. Forskolin is a plant-derived small-molecule activator of ACs; the natural activator or inhibitor of this site in the ACs has been postulated to exist (*20*) but so far has not been identified. In the case of AC9, we can now show that (i) forskolin is capable of activating the enzyme and (ii) the likely natural regulator of the allosteric site is the portion of the C2b domain binding to the active region of the protein. We suggest that, after activation by the G protein (fig. S14, A to D), C2b occludes the AC9 reaction center and blocks the enzymatic activity, preventing excessive production of cAMP in the cell (fig. S14E). This is consistent with a recent report on the autoinhibitory function of the AC9 C2b domain in a cellular context (*27*). Our findings may help pave the way toward generating new approaches in drug discovery that exploit the autoregulatory molecular mechanism revealed by the AC9-Gαs structure.

REFERENCES AND NOTES

1. R. K. Sunahara, C. W. Dessauer, A. G. Gilman, *Annu. Rev. Pharmacol. Toxicol.* **36**, 461–480 (1996).
2. W. J. Tang, A. G. Gilman, *Cell* **70**, 869–872 (1992).
3. D. Willoughby, D. M. Cooper, *Physiol. Rev.* **87**, 965–1010 (2007).
4. J. A. Allen *et al.*, *Mol. Pharmacol.* **76**, 1082–1093 (2009).
5. S. Pierre, T. Eschenhagen, G. Geisslinger, K. Scholich, *Nat. Rev. Drug Discov.* **8**, 321–335 (2009).
6. J. U. Linder, *Cell. Mol. Life Sci.* **63**, 1736–1751 (2006).

7. J. J. Tesmer, R. K. Sunahara, A. G. Gilman, S. R. Sprang, *Science* **278**, 1907–1916 (1997).
8. J. J. Tesmer *et al*., *Science* **285**, 756–760 (1999).
9. J. Krupinski *et al*., *Science* **244**, 1558–1564 (1989).
10. J. E. Schultz, S. Klumpp, R. Benz, W. J. Schürhoff-Goeters, A. Schmid, *Science* **255**, 600–603 (1992).
11. D. A. Baker, *IUBMB Life* **56**, 535–540 (2004).
12. I. Vercellino *et al*., *Proc. Natl. Acad. Sci. U.S.A.* **114**, E9821–E9828 (2017).
13. C. Gu, A. Sorkin, D. M. Cooper, *Curr. Biol.* **11**, 185–190 (2001).
14. R. T. Premont *et al*., *J. Biol. Chem.* **271**, 13900–13907 (1996).
15. Y. Li *et al*., *Sci. Rep.* **7**, 5522 (2017).
16. Y. Li, L. Chen, R. S. Kass, C. W. Dessauer, *J. Biol. Chem.* **287**, 29815–29824 (2012).
17. C. W. Dessauer, *Mol. Pharmacol.* **76**, 935–941 (2009).
18. K. G. Tantisira, K. M. Small, A. A. Litonjua, S. T. Weiss, S. B. Liggett, *Hum. Mol. Genet.* **14**, 1671–1677 (2005).
19. B. M. Hacker *et al*., *Genomics* **50**, 97–104 (1998).
20. S. Z. Yan, Z. H. Huang, R. K. Andrews, W. J. Tang, *Mol. Pharmacol.* **53**, 182–187 (1998).
21. R. Seifert, G. H. Lushington, T. C. Mou, A. Gille, S. R. Sprang, *Trends Pharmacol. Sci.* **33**, 64–78 (2012).
22. Y. Z. Chen *et al*., *Arch. Neurol.* **69**, 630–635 (2012).
23. F. C. Chang *et al*., *Mov. Disord.* **31**, 1033–1040 (2016).
24. S. R. Dharmaraj *et al*., *Ophthalmic Genet.* **21**, 135–150 (2000).
25. X. Zhao *et al*., *Mol. Vis.* **19**, 1039–1046 (2013).
26. S. G. Rasmussen *et al*., *Nature* **477**, 549–555 (2011).
27. A. Pálvölgyi *et al*., *Cell. Signal.* **51**, 266–275 (2018).

ACKNOWLEDGMENTS

We thank the PSI EM Facility (T. Ishikawa and E. Mueller-Gubler); the Center for Microscopy and Image Analysis at the University of Zurich; the Scientific Center for Optical and Electron Microscopy at ETH Zurich; and the Electron Microscopy Core Facility at EMBL Heidelberg. We acknowledge the European Synchrotron Radiation Facility for provision of beam time on CM01 (project MX 2106). We thank F. Weis (EMBL Heidelberg), M. Peterek (ETH Zurich), and E. Kandiah (ESRF) for support and expertise in high-resolution cryo-EM data collection. We also thank the scientific IT group at PSI (D. Ozerov) for support and M. Steinmetz (Paul Scherrer Institute) for critically reading and commenting on the manuscript. **Funding**: This study was supported by iNEXT (PID 3200), Swiss National Science Foundation (SNF Professorship 150665), ETH (ETH-29 15-1), and Novartis Foundation for Medical-Biological Research (14C178) grants to V.M.K. and Swiss National Science Foundation (SNSF 31003A_179418) and Mäxi Foundation grants to O.M. **Author contributions**: C.Q. designed and performed the experiments, analyzed the data, and wrote the manuscript; S.S. performed the cryo-EM data collection experiments and contributed to writing the manuscript; O.M. designed the experiments and contributed to writing the manuscript; and V.M.K. designed the experiments, analyzed the data, and wrote the manuscript. **Competing interests**: The authors declare no competing interests. **Data and materials availability**: The cryo-EM density maps have been deposited in the Electron Microscopy Data Bank with accession numbers EMD-4719, EMD-4721, EMD-4722, EMD-4723, EMD-4724, EMD-4725, and EMD-4726. The atomic coordinates have been deposited in the Protein Data Bank with entry codes 6R3Q, 6R4O, and 6R4P. All other data are available in the manuscript or the supplementary materials.

SUPPLEMENTARY MATERIALS

science.sciencemag.org/content/364/6438/389/suppl/DC1
Materials and Methods
Figs. S1 to S14
Tables S1 and S2
References (*28*–*47*)

11 August 2018; resubmitted 2 February 2019
Accepted 26 March 2019
10.1126/science.aav0778

Science

The structure of a membrane adenylyl cyclase bound to an activated stimulatory G protein

Chao Qi, Simona Sorrentino, Ohad Medalia and Volodymyr M. Korkhov

Science **364** (6438), 389-394.
DOI: 10.1126/science.aav0778

The architecture of a signaling hub

Adenylyl cyclases (ACs) respond to a variety of inputs to generate the signaling molecule cyclic adenosine monophosphate. ACs are regulated by G proteins, which are activated by upstream receptors. Qi *et al.* determined the structure of bovine membrane AC9 bound to an activated G protein αs subunit by cryo–electron microscopy at 3.4-angstrom resolution. The structure provides the full architecture of AC9, including a helical domain that connects the transmembrane and catalytic domains. The model reveals how the domains interact to regulate enzymatic activity, including suggesting a mechanism of self-inhibition.

Science, this issue p. 389